Macromolecules

ARTICLE

pubs.acs.org/Macromolecules

Controlling the Orientation of Block Copolymer Thin Films using Thermally-Stable Gold Nanoparticles with Tuned Surface Chemistry

Misang Yoo,[†] Seyong Kim,[†] Se Gyu Jang,[⊥] Soo-Hyung Choi,[⊥] Hyunseung Yang,[‡] Edward J. Kramer,[⊥,∥] Won Bo Lee,[*,§] Bumjoon J. Kim,[*,‡] and Joona Bang[*,†]

[†]Department of Chemical and Biological Engineering, Korea University, Seoul 136-701, Republic of Korea

[‡]Department of Chemical and Biomolecular Engineering, Korea Advanced Institute of Science and Technology (KAIST), Daejeon 305-701, Republic of Korea

[§]Department of Chemical and Biomolecular Engineering, Sogang University, Seoul 121-742, Republic of Korea

[⊥]Department of Materials and the Materials Research Laboratory, University of California, Santa Barbara, California 93106, United States

[∥]Department of Chemical Engineering, University of California, Santa Barbara, California 93106, United States

Supporting Information

ABSTRACT: In this study, we developed a novel strategy to control the orientation of microdomains in block copolymer thin films by introducing either selective or neutral gold nanoparticles (Au NPs) that were thermally stable. The Au NPs were modified with thiol-terminated polymeric ligands, poly[(methyl methacrylate-*r*-styrene)-*b*-azidostyrene] (P[(MMA-*r*-S)-*b*-S-N_3]-SH), having different compositions of methyl methacrylate (MMA) and styrene in P(MMA-*r*-S) block to precisely tune the interfacial interaction between the Au NPs and block copolymer template, poly(styrene-*b*-methyl methacrylate) (PS-*b*-PMMA). These Au NPs have a cross-linked polymeric shell, via UV cross-linking of P(S−N_3) block, and thus were stable under thermal annealing at temperatures up to ∼200 °C. The selective Au NPs, which had 80 mol % PMMA in the P(MMA-*r*-S) block, were located within the PMMA domain of the PS-*b*-PMMA block copolymer. In contrast, the neutral Au NPs, which had 20 mol % PMMA in the P(MMA-*r*-S) block, were localized at the interface between the PS and PMMA blocks of the PS-*b*-PMMA. When these Au NPs were incorporated into PS-*b*-PMMA thin films, these different locations of Au NPs resulted in a remarkable difference in orientation of the block domains. When the selective Au NPs were added and were located in the PMMA domains, the microdomains were oriented parallel to the substrate. In contrast, when the neutral Au NPs that localize at the block copolymer interfaces were added, they induced a transition in the orientation of microdomains from parallel to perpendicular to the substrate. The lateral and vertical location of the Au NPs in the film was investigated by top-view and cross-sectional transmission electron microscopy (TEM). Also, we employed self-consistent mean field theory (SCFT) simulations to explain our experimental results.

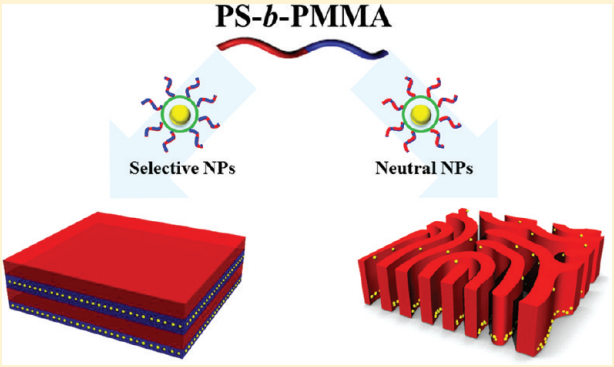

INTRODUCTION

In nanotechnology, the fabrication of high quality, small scale features is often a primary goal and various top-down and bottom-up methods with different capabilities have been developed. Among these, the self-assembly of block copolymers has been received considerable attention, as such self-assembly can produce features with length scales of tens of nanometers. The length scale of features and their morphology can be tuned by controlling the molecular weight and composition of the block copolymer.[1−5] This bottom-up method can be combined with top-down technologies such as UV or electron beam lithography to register the block copolymer pattern to underlying features on a substrate.[6−10] Such block copolymer nanotemplates can have wide applications including microelectronic devices, high density magnetic memories, nanowire transistors, membranes and biosensors.[11−17] The incorporation of metal nanoparticles (NPs) into a block copolymer template can allow for the formation of multifunctional thin films with structures and properties beyond those possible with just the block copolymer or the nanoparticles alone.[18−26] Metal NPs can contribute properties such as electrical and thermal conductivity, mechanical stiffness, and optical and magnetic properties as well as catalytic activity that organic materials do not have. To capitalize on the properties of NPs, accurate control of the placement of these NPs is critical.[27,28]

Received: August 23, 2011
Revised: October 10, 2011
Published: November 10, 2011

For this purpose, block copolymers are promising because their ordered self-assembled structures can act as a template for the placement of NPs.[1,2] However, bare metal NPs are difficult to disperse in block copolymers due to their high interfacial energy, which causes the NPs to aggregate and disperse poorly in the block copolymer domains.

One of the most important developments for improving the compatibility and stability of metal or inorganic NPs is to modify their surfaces with polymeric ligands.[29−31] The chemical composition, molecular weight and grafting density of the ligand can influence not only the location and dispersion of the NPs but also the final morphology of the nanocomposites.[32−40] Kim et al. were able to control the location of gold (Au) NPs by varying the brush type, grafting density and chain length of polymeric ligands within a poly(styrene-*b*-2-vinylpyridine) (PS-*b*-P2VP) diblock copolymer.[41−47] They also found that the location and concentration of Au NPs can affect the ultimate morphology of the block copolymers.[41,48] However when the block copolymer nanocomposites are prepared in the form of thin films, the orientation of microdomains with respect to the substrates is also required.

In this respect, there are a few examples demonstrating that NPs can be used to direct the orientation of block copolymer microdomains. Theoretically, Balazs and co-workers examined the morphology of confined copolymer/NPs mixtures. They used a mixed approach using self-consistent mean field theory (SCFT) for diblock copolymers and density functional theory (DFT) for particles, which yields a SCFT/DFT model for nanocomposites.[49] In their study, the symmetric diblock copolymer formed parallel-oriented lamellae at equilibrium on a substrate that has a low interfacial energy with only one of the blocks. But after adding neutral NPs to the block copolymer thin film, the orientation of the block copolymer changed from parallel to perpendicular. On the basis of these findings, they suggested that the neutral NPs were located at the interface of the self-assembled block copolymer domains and were near the substrate to reduce the entropy loss of the polymer chains. In addition, it was reported that these NPs reduce the interfacial tension and neutralize the substrate so that the neutral NPs induced a perpendicular orientation of the block copolymer. Experimentally, Russell and co-workers demonstrated that NPs can play a role in directing the orientation of microdomains by mediating the interfacial interactions.[32] In that work, they incorporated cadmium selenide (CdSe) NPs covered by tri-n-octylphosphine oxide ligands into cylindrical PS-*b*-P2VP block copolymers to obtain the perpendicular orientation of P2VP cylinders on silicon wafers after thermal annealing. The CdSe nanoparticles were segregated to the surface of the film within the P2VP cylinders. Recently, we reported that an addition of hydrophilic Au NPs into poly(styrene-*b*-methyl methacrylate) (PS-*b*-PMMA) can also direct the orientation of microdomains via a solvent annealing process.[36] In this case, the majority of hydrophilic Au NPs are within the cylindrical PMMA domain, and they interact with water vapor at the film surface during the solvent annealing process, thereby, leading to the perpendicular orientation of PMMA cylinders. Although these examples certainly demonstrated the active role of NPs in directing the orientation of microdomains in block copolymer thin films, the exact mechanisms with respect to Balazs' simulations have not been shown.

To elucidate the mechanism of the effect of NPs on the orientation of microdomains, the system needs to be carefully designed. First, two types of NPs, one selective for one of the domains and one type that is nonselective as shown by its segregation to the block copolymer interface, should be prepared. This can be done by synthesizing polymeric ligands having different compositions. Second, it is desirable that the NPs and block copolymer nanocomposites are thermally processed to obtain equilibrium morphologies and hence the NPs require thermal stability. However, it is well-known that the most NPs suffer from the low thermal stability due to the dissociation of the ligands, especially the convenient end-functional thiol ligands, from the NPs at elevated temperature. To impart the thermal stability of NPs, we previously reported the synthesis of thermally stable core−shell Au NPs using UV cross-linkable block copolymer ligands, P(S-*b*-S-N_3)-SH.[50,51] After UV cross-linking of the P(S−N_3) block, the resulting Au NPs have a thin inner layer of a cross-linked shell with an outer un-cross-linked PS brush. These Au NPs exhibited excellent thermal stability under exposure to temperatures above 200 °C. Furthermore, it was also shown that these Au NPs were segregated along the interface of PS and PMMA blends, as the outer, nonpolar PS brush and the inner, polar cross-linked shell have a roughly balanced interaction with the PS and PMMA domains. By varying the composition of PS or P(S−N_3) block in the ligand, the surface properties of the NPs can be readily controlled while maintaining their thermal stability. Therefore, we believe that this system is ideal for examining the equilibrium morphology of NPs and block copolymer nanocomposites.

In this work, we investigate the effect of Au NPs on the orientation of microdomains in PS-*b*-PMMA thin films after thermal annealing by designing two types of thermally stable Au NPs, one that is selective to one domain and the other that is nonselective. To control the interfacial interaction between the PS-*b*-PMMA block copolymer and Au NPs, we further tuned the surface properties of the thermally stable Au NPs by adjusting the composition of PS and PMMA in the ligands during synthesis. Two kinds of NPs that interacted differently with PS and PMMA produced quite different effects on the orientation of PS-*b*-PMMA thin films. Interestingly, the addition of nonselective Au NPs causes a dramatic change in the orientation of the PS-*b*-PMMA morphology from parallel to perpendicular to the substrate. We also compared SCFT simulation results between two flat walls with a nanoparticle located in either parallel- or perpendicular-oriented diblock copolymer lamellae. These simulations showed that the perpendicular lamellae with particles located at the wall have the lowest free energy in agreement with our experimental results.

EXPERIMENTAL SECTION

Synthesis of Polymeric Ligands. The thiol-terminated polymeric ligands were synthesized via reversible addition−fragmentation transfer (RAFT) polymerization as previously described.[50] For P[(MMA-*r*-S)-*b*-S-N_3]-SH (ligand 1), styrene (3.12 g, 0.03 mol), methyl methacrylate (12.01 g, 0.12 mol), RAFT agent (0.69 g, 2.3 mmol) and 2,2′- azobis(isobutyronitrile) (AIBN) (0.037 g, 0.23 mmol) were mixed and purged with nitrogen gas in a Schlenk flask. The polymerization was performed at 70 °C for 6 h. The viscous mixture was dissolved in dichloromethane and precipitated into methanol to produce poly(methyl methacrylate-*r*-styrene) as a pink solid. The molecular weight (M_n) of poly(methyl methacrylate-*r*-styrene) was 2100 g/mol. The poly(methyl methacrylate-*r*-styrene) (2.3 g, 1.1 mmol) was then dissolved in benzene with 4-vinylbenzyl chloride (S−Cl) (3.3 g, 20.6 mmol), AIBN (0.018 g, 0.11 mmol) and purged with nitrogen gas. The second polymerization step was performed at 70 °C for 10 h. The

mixture was then dissolved in dichloromethane and precipitated into methanol to produce P[(MMA-*r*-S)-*b*-S-Cl]. The molecular weight M_n and polydispersity index (PDI) of P[(MMA-*r*-S)-*b*-S-Cl] were 2800 g/mol and 1.20, respectively. The P[(MMA-*r*-S)-*b*-S-Cl] was then dissolved in dry THF with hexylamine and purged with nitrogen gas. The substitution reaction was performed at room temperature overnight. The mixture was precipitated into methanol to produce thiol-terminated P[(MMA-*r*-S)-*b*-S-Cl]-SH as a white solid powder. The polymer was then mixed with 4 equiv of sodium azide in dimethylformamide under ambient conditions for 24 h. The resulting P[(MMA-*r*-S)-*b*-S-N_3]-SH was precipitated into methanol and dried in vacuo. The other ligands, ligands 2−4, were synthesized using the same procedure described above but with a different feed mole ratio of styrene and methyl methacrylate for the first polymerization step.

Synthesis of Thermally Stable Gold Nanoparticles. The synthesis of P[(MMA-*r*-S)-*b*-S-N_3]-SH coated Au NPs was accomplished using the two-phase method. The feed mole ratio of the polymer ligand to Au atoms was 0.3. The polymer coated Au NPs were separated from unattached polymer and residues by ultrafiltration membrane (MWCO 30 000 Da, Millipore, Inc.) using dimethylformamide (DMF) as a solvent several times and concentrated by centrifugation to produce a dark purple powder. To impart thermal stability via cross-linking, the Au NPs were dispersed in dioxane and the solutions were exposed to the UV light (λ = 254 nm) for 1 h under ambient conditions using a hand UV lamp (intensity of ~2 mW/m^2). The cross-linked Au NPs were separated by centrifugation and dried in vacuo overnight.

Preparation of Nanocomposite Bulk. A 2 wt % dichloromethane solution of lamellar forming PS-*b*-PMMA (M_n = 94 kg/mol and PDI = 1.09, M_n = 130 kg/mol and PDI = 1.08, Polymer Source Inc.) was mixed with 10 wt % of cross-linked Au NPs relative to the polymer. The nanocomposites in the bulk state were prepared by drop casting the solution on the NaCl substrates and annealed at 200 °C for 48 h. For transmission electron microscopy analysis, the films were floated by removing the NaCl substrate on DI water and then transferred to an epoxy support. Embedded films were microtomed into a section several tens of nanometers thick. PS domains were stained with RuO_4.

Preparation of Nanocomposite Thin films. A toluene solution of PS-*b*-PMMA (M_n = 94 kg/mol and PDI = 1.09; M_n = 130 kg/mol and PDI = 1.08, Polymer Source Inc.) was mixed with cross-linked Au NPs to produce a weight fraction of NPs of 1.0, 5.0, and 10.0 wt % relative to the block copolymer. The nanocomposite thin films were spin coated from the toluene solution onto silicon substrates without a neutral layer. The film thickness was adjusted by controlling the solution concentration and the spin rate. The 94k PS-*b*-PMMA thin films were annealed at 190 °C for 4 days and 130k PS-*b*-PMMA thin films were annealed at 200 °C for 7 days in a vacuum.

Top-View and Cross-Sectional TEM of Nanocomposites Thin Films. To obtain top-view TEM images, the annealed thin films were lifted off by etching the silicon oxide layer from the substrate with a dilute hydrogen fluoride (HF) solution. The films were then transferred to a copper grid and the PS domains were selectively stained using RuO_4. To obtain cross-sectional TEM images, 90−100 nm-thick nanocomposite thin films composed of 94k or 130k PS-*b*-PMMA and 10 wt % of Au NPs-1 and Au NPs-3 were prepared and annealed under the same conditions described above. Amorphous carbon multilayers were sputtered on the nanocomposite thin films first, then the thin films were lifted off with HF and placed upside down on epoxy resin. The bottom side of the thin films was coated by a gold layer using gold sputter and covered with epoxy resin. Finally, the nanocomposite thin films were microtomed with a thickness of several tens of nm and the PMMA domains were selectively stained using OsO_4.

SCFT Calculations. The diblock copolymers are described as Gaussian (flexible) chains, and a particle is modeled as a cavity field function. Dissimilar segments and particles interact locally via Flory type

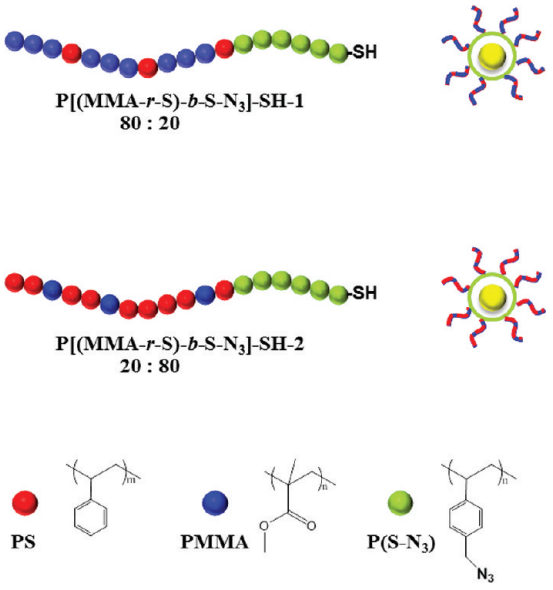

Figure 1. Schematic illustration of synthesis of polymeric ligands and PMMA selective thermally stable Au NPs (top) and neutral Au NPs (bottom) which are coated by two different types of P[(MMA-*r*-S)-*b*-S-N_3]-SH polymeric ligands.

interactions (χN), and an incompressiblility constraint is enforced. We assumed that both wall and particles are neutral. The pairwise interactions between two diblock segments (A/B) are set to be $\chi_{AB}N$ = 20. We fixed the particle diameter (D_p) divided by the bulk lamella spacing (D_{bls}), D_p/D_{bls} = 0.123. The SCFT equations were solved numerically.[52−56]

RESULTS AND DISCUSSION

As illustrated in Figure 1, we prepared thermally stable gold nanoparticles (Au NPs) having various surface property. In this case, the surface chemistry of Au NPs was controlled by using thiol-terminated polymeric ligands with varying composition of PS and PMMA. These were synthesized via reversible addition−fragmentation chain transfer (RAFT) polymerization as described previously (see Supporting Information, Figure S1).[50] To tune the surface properties of Au NPs, the outer brush part was made up of a random copolymer of PMMA and PS, P(MMA-*r*-S), whose composition could be tuned so that the Au NPs would have the desired interaction with the PS and PMMA domains of the block copolymer. From our previous report, it was found that Au NPs coated with P(S-*b*-S-N_3)-SH, having pure PS in the outer brush part, were located at the PS/PMMA interface of PS and PMMA blends due to the balanced interaction of nonpolar PS brush and polar P(S−N_3) inner shell with PS and PMMA domains. Therefore, we designed the selective Au NPs as PMMA selective by increasing the composition of PMMA in the outer shell, P(MMA-*r*-S) block, while keeping the polar P(S−N_3) block for shell cross-linking.

As a consequence, we varied the compositions of P(MMA-*r*-S) brush as 80 mol % MMA, 50 mol % MMA, 20 mol % MMA, and 0 mol % MMA. The molecular weights (M_n) of both random copolymer blocks were controlled to be ~2000 g/mol. To improve thermal stability, the P(S−N_3) block (~700 g/mol) was polymerized as a second block. The resulting polymeric ligands, P[(MMA-*r*-S)-*b*-S-N_3]-SH, that have a PMMA/PS composition of 80:20, 50:50, 20:80, and 0:100 are denoted as

Table 1. Summary of the Molecular Weight, Polydispersity Index, and Feed Mole Ratio of the Synthesized Polymeric Ligands for the Au NPs Surface Modification

				feed mole ratio in P(MMA-*r*-S)	
	P(MMA-*r*-S) M_n (g/mol)	total M_n (g/mol)	PDI	MMA	styrene
P[(MMA-*r*-S)-*b*-S-N_3]-SH-1 (ligand 1)	2100	2800	1.20	80	20
P[(MMA-*r*-S)-*b*-S-N_3]-SH-2 (ligand 3)	2000	2800	1.21	50	50
P[(MMA-*r*-S)-*b*-S-N_3]-SH-3 (ligand 3)	2300	3000	1.19	20	80
P(S-*b*-S-N_3)-SH-4 (ligand 4)	2000	2900	1.11	0	100

ligand-1, ligand-2, ligand-3, and ligand-4, respectively. For 100 mol % PMMA, it should be noted that they were not successfully prepared because the second P(S−N_3) block is not added to PMMA-RAFT. Also, during UV cross-linking of P(S−N_3) block, it is likely that the pure PMMA brush can be also damaged by UV, while it is well-known that a small fraction of PS in the P(S-*r*-MMA) can efficiently suppress the photodegradation.[57,58] The M_n of the random block and the entire polymeric ligands, the polydispersity index (PDI) and feed mole ratio in P(MMA-*r*-S) are summarized in Table 1. (also see the NMR spectra in Supporting Information, Figure S2) The ligands coated Au NPs were synthesized via two-phase method[42,58,59] and they are denoted as Au NPs-1, Au NPs-2, Au-NPs-3, and Au-NPs-4, respectively. To remove unbound polymeric ligands and residual agents, Au NPs were washed several times with dimethylformamide (DMF) using an ultrafiltration membrane. Then, they were dispersed in dioxane and irradiated with the UV light (λ = 254 nm) for 1 h to cross-link the P(S−N_3) shell, resulting in the formation of thermally stable core−shell Au NPs.[24,58] The diameters of these Au NPs core were less than 3 nm, as measured by transmission electron microscopy (TEM) (see Supporting Information, Figure S3).

To examine the location of these Au NPs within the PS-*b*-PMMA block copolymer templates, we prepared the PS-*b*-PMMA nanocomposites in the bulk consisting of 10 wt % Au NPs relative to PS-*b*-PMMA. Two types of lamellar forming PS-*b*-PMMA block copolymers, one with M_n = 94 kg/mol (PS volume fraction, f_{PS} = 0.56) and PDI = 1.09, and, the other with M_n = 130 kg/mol (f_{PS} = 0.54) and PDI = 1.08, were used (Polymer Source Inc.). The bulk samples were prepared by drop casting from the 2 wt % DCM solution of PS-*b*-PMMA/Au NPs onto an NaCl substrate and then annealing at 200 °C for 2 days in a vacuo. These thick bulk samples were transferred to a partially cured epoxy underlayer after dissolving the sacrificial NaCl substrate. These samples were covered with epoxy which was allowed to cure and then microtomed into 50−100 nm thick slices for TEM analysis. The PS domains were stained selectively with RuO_4. Figure 2 shows the cross-sectional TEM images of 130 kg/mol PS-*b*-PMMA containing four different Au NPs. From Figures 2a and 2b, it is apparent that most of the Au NPs-1 and Au NPs-2 were located at the center of the PMMA domain (lighter region) due to their preferential interaction with PMMA, whereas the Au NPs-3 were located at the interface of the PS and PMMA domain (Figure 2c) due to a neutral interaction between Au NPs and PS/PMMA. Therefore, it can be concluded that the Au NPs-1 and Au NPs-2 were selective to PMMA and Au NPs-3 were neutral to PS and PMMA. Comparing the Au NPs distribution from the histograms, it is clear that Au NPs-1 is more selective to PMMA than Au NPs-2, as they are clearly localized at the center of PMMA domain. From Figure 2d, it is interesting that Au NPs-4 were mainly located at the PS domain with some of Au NPs at the interface, although it was previously observed that the same Au NPs localized at the interface in the PS and PMMA blend system.[50] We attribute such different behavior to an extra entropy penalty imposed by the chain connectivity of block copolymer interface. Therefore, in the block copolymer, more adsorption energy is required for Au NPs to precisely locate at the interface. As a consequence, we found that the optimal compositions of P(MMA-*r*-S) brush are 80 mol % MMA and 20 mol % S for PMMA selective Au NPs, i.e., Au NPs-1, and 20 mol % MMA and 80 mol % S for neutral Au NPs, i.e., Au NPs-3. Similarly, in the case of the 94 kg/mol PS-*b*-PMMA, it was observed that the Au NPs-1 were also located in the PMMA domain and Au NPs-3 were segregated at the PS/PMMA interface as was observed for 130 kg/mol PS-*b*-PMMA (see Supporting Information, Figure S4). It is worth noting that the neutral characteristics of Au NPs was achieved when the PMMA and PS composition of P(MMA-*r*-S) brush was adjusted to 20:80, not ∼40:60, which is the well-known neutral composition of PS and PMMA in the flat surface.[60,61] This can be attributed to the presence of the polar nitrogens in aziridine or diazo cross-links after photolysis of the inner P(S−N_3) shells.[24] Previously, it was demonstrated that Au NPs coated with P(S-*b*-S-N_3)-SH, consisting of nonpolar, outer PS brush and polar, inner cross-linked P(S−N_3) shell can have a balanced interaction with PS and PMMA blends, and thus they are located at the interface of PS/PMMA binary blends.[50] Similarly, the balanced interaction in the block copolymer system in the current experiments was obtained with higher PS composition in the outer P(MMA-*r*-S) brush due to the polar, inner shell of cross-linked P(S−N_3) block.

To further investigate the effect of the NPs location on the PS-*b*-PMMA thin film morphologies, PS-*b*-PMMA/Au NPs thin-films were fabricated with various amounts of Au NP-1 or Au NP-3. A 1.5 wt % toluene solution of 94 kg/mol PS-*b*-PMMA was mixed with 1, 5 and 10 wt % of Au NPs-1 or Au NPs-3 relative to the PS-*b*-PMMA. The nanocomposite thin films were prepared by spin-casting onto silicon substrates. It should be noted that the silicon substrates were not neutralized with P(S-*r*-PMMA) random copolymers.[60,61] The thickness of the nanocomposite thin films was controlled as ∼50 nm. All samples were then annealed at 190 °C for 4 days in vacuo. Parts a−c of Figure 3 show the scanning force microscopy (SFM) height images of PS-*b*-PMMA nanocomposite thin films containing 1, 5 and 10 wt % of selective Au NPs-1, respectively, and parts d−f of Figure 3 correspond to the SFM height images of the PS-*b*-PMMA nanocomposite thin films containing 1, 5, and 10 wt % of neutral Au NPs-3, respectively. In the case of the nanocomposite thin films containing the Au NPs-1, which were selective to the PMMA, lamellar forming PS-*b*-PMMA thin films were oriented

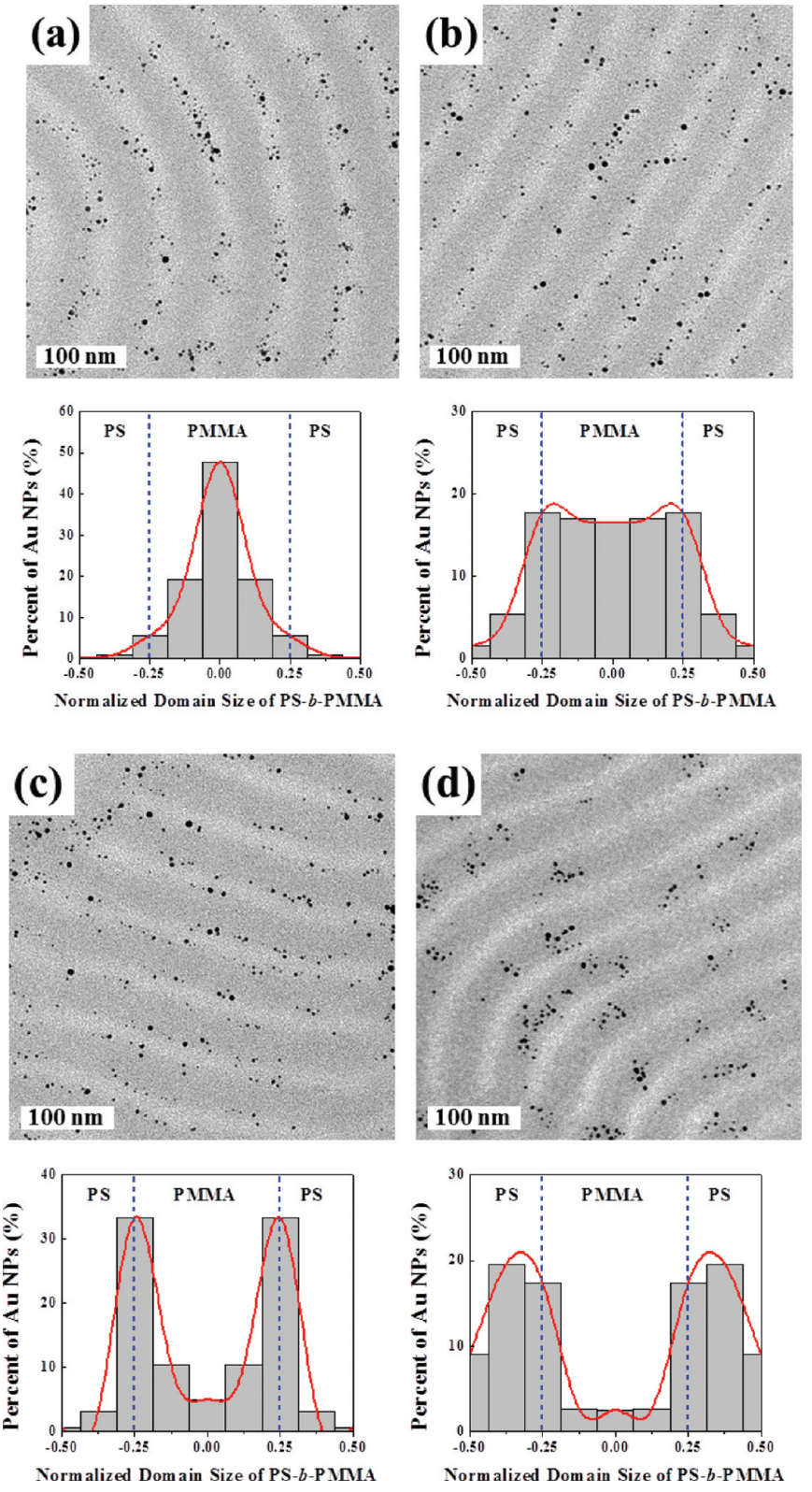

Figure 2. Cross-sectional TEM images and the corresponding histograms of nanoparticle location in nanocomposites consisting of PS-*b*-PMMA (M_n = 130 kg/mol) and (a) 10 wt % of Au NP-1, (b) 10 wt % of Au NP-2, (c) 10 wt % of Au NP-3, and (d) 10 wt % of Au NP-4 after annealing at 200 °C for 2 days. PS domains are stained selectively by RuO_4.

parallel to the substrate, as evidenced by the typical hole and island patterns regardless of Au NPs concentrations. Therefore, it can be seen that the selective Au NPs, which were located in the PMMA domain, did not affect the morphology and orientation of the PS-*b*-PMMA thin films compared to those of pure PS-*b*-PMMA thin films on the silicon substrate whose thin SiOx layer

dx.doi.org/10.1021/ma2019254 |*Macromolecules* 2011, 44, 9356–9365

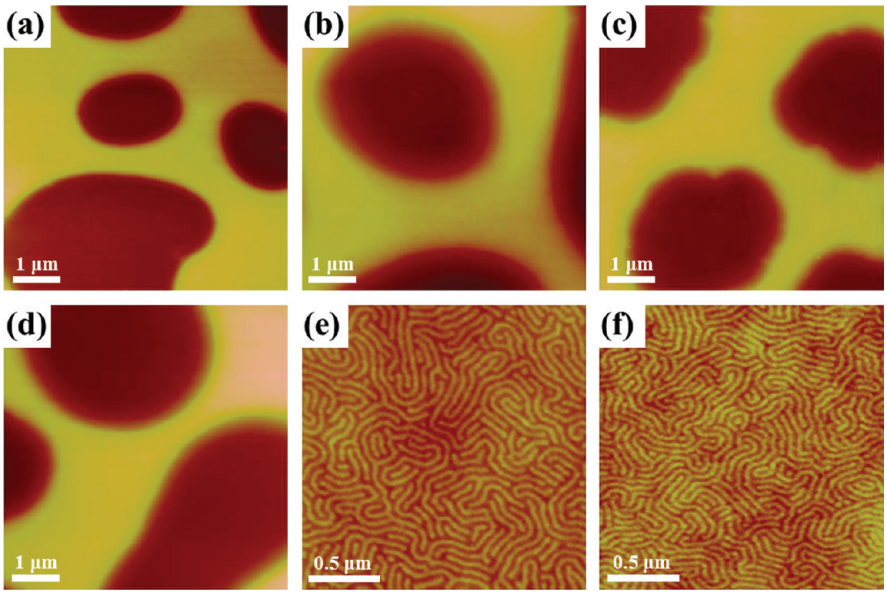

Figure 3. SFM height images of PS-*b*-PMMA (M_n = 94 kg/mol) nanocomposite thin films (thickness: ~ 50 nm) containing (a) 1 wt %, (b) 5 wt %, (c) 10 wt % of Au NP-1 and (d) 1 wt %, (e) 5 wt %, (f) 10 wt % of Au NP-3 respectively. The height scales are Δz = 0−100 nm (a−d) and Δz = 0−15 nm (e and f). All samples were annealed at 190 °C for 4 days in vacuo.

hydrogen bonds through its surface silanol groups selectively to the PMMA domain. In contrast, an incorporation of neutral Au NPs-3 into the PS-*b*-PMMA thin films caused a dramatic change in the thin film morphology. When 1 wt % of neutral Au NPs-3 were added, the PS-*b*-PMMA thin film exhibited the parallel orientation of microdomains as in the case of the selective Au NPs-1. However, with an increasing amount of Au NPs-3, 5, and 10 wt %, the microdomains were oriented perpendicular to the substrate, as shown by the fingerprint patterns (Figure 3, parts e and f). This suggests that above a certain threshold amount (<5 wt %) of neutral Au NPs, the preferential interaction between the PMMA block of the block copolymer and the substrate is overcome, thereby inducing a perpendicular orientation of the PS-*b*-PMMA thin film. The ordering and orientation of 94 kg/mol PS-*b*-PMMA nanocomposite thin films was also examined using grazing incidence small-angle X-ray scattering (GISAXS) that was measured at the 4C2 beamline at the Pohang Accelerator Laboratory (PAL), Korea (see Supporting Information, Figure S5). In the intensity profiles scanned at a constant q_z = 0.189 nm^{-1}, the relative scattering vector of the four peaks was determined to be 1:2:3:4, which was dictated by the perpendicular orientation of lamellar forming microdomains with good lateral ordering. To examine the morphologies of PS-*b*-PMMA/Au NPs thin films for all samples in Figure 3 as a function of film thickness, we increased the film thickness to ~100 nm by adjusting the solution concentration and annealed the film at 190 °C for 4 days in vacuo (see Supporting Information, Figure S6). Although the film thickness was changed, the overall morphologies of the nanocomposite thin films were same as when the thickness was ~50 nm. At all Au NPs concentrations, the Au NPs-1 had no effect on the morphology of the PS-*b*-PMMA thin film and all films were oriented parallel to the substrate. However, a perpendicular orientation was clearly observed for the thicker PS-*b*-PMMA nanocomposite thin films containing 5 wt % or more of neutral Au NPs-3.

We also investigated the thin film orientation using higher M_n of PS-*b*-PMMA (M_n = 130 kg/mol). A 2.5 wt % toluene solution of PS-*b*-PMMA was mixed with 1, 5 and 10 wt % of Au NPs-1 or Au NPs-3 relative to the PS-*b*-PMMA. The nanocomposite thin films were prepared by spin-casting onto a silicon wafer with a native SiO_x surface. The resulting films have a thickness of ~100 nm and were annealed at 200 °C for 7 days in vacuo. Figure 4 shows the SFM height images of the 130 kg/mol PS-*b*-PMMA nanocomposite thin films with various amounts of Au NPs-1 or Au NPs-3. The overall morphologies of the PS-*b*-PMMA thin films were same as the case of the 94 kg/mol PS-*b*-PMMA nanocomposite films. Regardless of NP concentration, the PS-*b*-PMMA thin films containing selective Au NPs-1 were oriented parallel to the substrate. However, the PS-*b*-PMMA thin films containing 5 wt % and 10 wt % of neutral Au NPs-3 were oriented perpendicular to the substrate.

To better understand why the neutral Au NPs can induce the perpendicular orientation of PS-*b*-PMMA thin films, the lateral and vertical location of the Au NPs within the thin films was examined by top-view and cross-sectional TEM. To obtain cross-sectional TEM images, 94 kg/mol or 130 kg/mol PS-*b*-PMMA nanocomposite thin films containing 10 wt % Au NPs were prepared. Amorphous carbon multilayers were sputtered on the nanocomposite thin films first and then the thin films were lifted off with HF, and then placed upside down on an epoxy resin. The bottom side of the thin films was coated by a sputtered deposited gold layer and covered with epoxy resin which was subsequently cured. Finally, the embedded nanocomposite thin films were microtomed to produce slices with a thickness of several tens of nanometers, and the PMMA domains were selectively stained using OsO_4. Figure 5 exhibits the top-view TEM images of 94 kg/mol and 130 kg/mol lamellar forming PS-*b*-PMMA nanocomposite thin films containing 10 wt % of neutral Au NPs showing the perpendicular orientation. The film morphologies are consistent with the SFM images in Figures 3f and 4f and the Au NPs can be identified as dark spots. As seen from the TEM images of bulk samples for Au NPs-3/PS-*b*-PMMA nanocomposites in Figure 2, parts a and c, one can expect that Au NPs are located at the PS/PMMA interface. However, in thin films, it can be seen

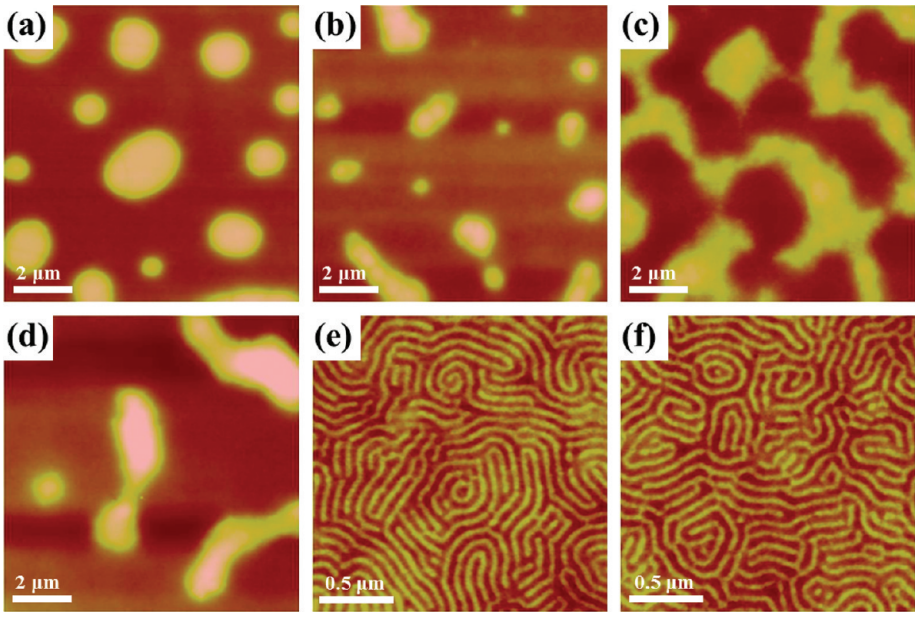

Figure 4. SFM height images of PS-*b*-PMMA (M_n = 130 kg/mol) nanocomposite thin films (thickness: ~ 100 nm) containing (a) 1 wt %, (b) 5 wt %, and (c) 10 wt % of Au NP-1 and (d) 1 wt %, (e) 5 wt %, and (f) 10 wt % of Au NP-3, respectively. The height scales are Δz = 0−70 nm (a−d) and Δz = 0−10 nm (e and f). All samples were annealed at 200 °C for 7 days in vacuo.

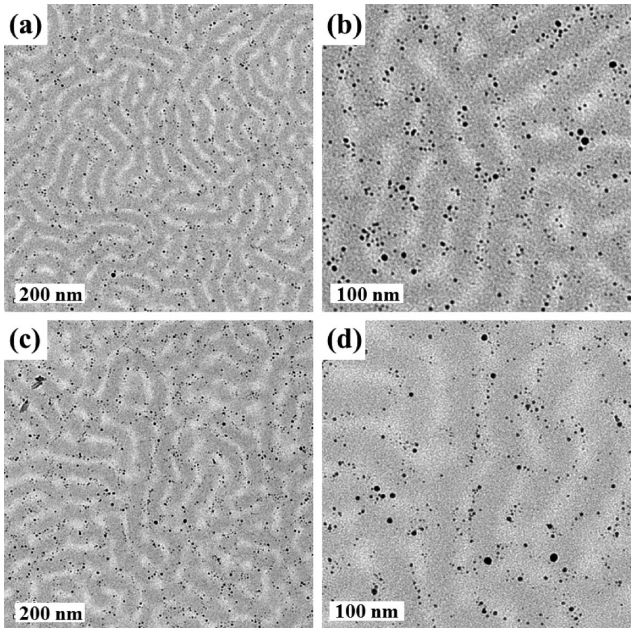

Figure 5. TEM images (top view) of (a, b) PS-*b*-PMMA (M_n = 94 kg/mol) nanocomposite thin films containing 10 wt % of Au NP-3 and (c, d) PS-*b*-PMMA (M_n = 130 kg/mol) nanocomposite thin films containing 10 wt % of Au NP-3. PS domains are stained selectively by RuO_4.

that Au NPs are well dispersed throughout the whole domains, rather than localized at the interface. In the higher magnification images (Figure 5, parts b and d), a considerable amount of Au NPs-3 can be found at the PS/PMMA interface but not sharply segregated as the case of the bulk samples (Figure 2). Such dispersity of Au NPs in thin films can be attributed to the relocation of NPs from the interface between the PS and PMMA blocks to the boundary with the silicon substrate. The neutral Au NPs are located at the PS/PMMA interface due to the balanced enthalpic interactions, but, at the same time, they distort the chains of the surrounding block copolymers near the interface and thus incur an entropic penalty. In the thin films, the entropic penalty of NPs can be reduced by moving these toward the substrate, and thus the perpendicular orientation of microdomains should be more favorable since it allows the nanoparticles to readily diffuse to the substrate. When the NPs move to the substrate, they can be distributed to mediate the interaction of the substrate with both domains and in doing so also reduce the conformational entropy penalty of polymer chains near the substrate. The SCFT simulations in the last section support this view.

To investigate the vertical location of Au NPs, Figure 6 shows representative cross-sectional TEM images of 94 kg/mol and 130 kg/mol lamellar forming PS-*b*-PMMA thin film containing 10 wt % of selective Au NPs-1 and neutral Au NPs-3. For the nanocomposite thin film containing Au NPs-1, the PS-*b*-PMMA domains were oriented parallel to the substrate and the Au NPs-1 were mainly located in the PMMA microdomains. In the case of the nanocomposite thin film containing Au NP-3, the PS-*b*-PMMA thin films clearly show the perpendicular orientation of the block microdomains as shown by vertical stripes throughout the thickness of thin films. In this case, the neutral Au NPs-3 were mainly located near the bottom surface and some of Au NPs were also located near the top surface. As mentioned above, we believe that the neutral Au NPs were pushed toward substrate to reduce the entropic penalty, and thus these NPs can neutralize the surface and induce the perpendicular orientation of microdomains.

To gain further insight into this change in PS-*b*-PMMA orientation by addition of neutral Au NP-3, the effect of the particle location on block copolymer orientation in the thin film was investigated by SCFT simulations. Unlike the SCFT/DFT model of Balazs et al.,[49] here a cavity field was used to represent a particle. The cavity field guarantees that there is no penetration of the diblock copolymers into a particle. To explain the behavior of the particles, the free energy and entropy were investigated at

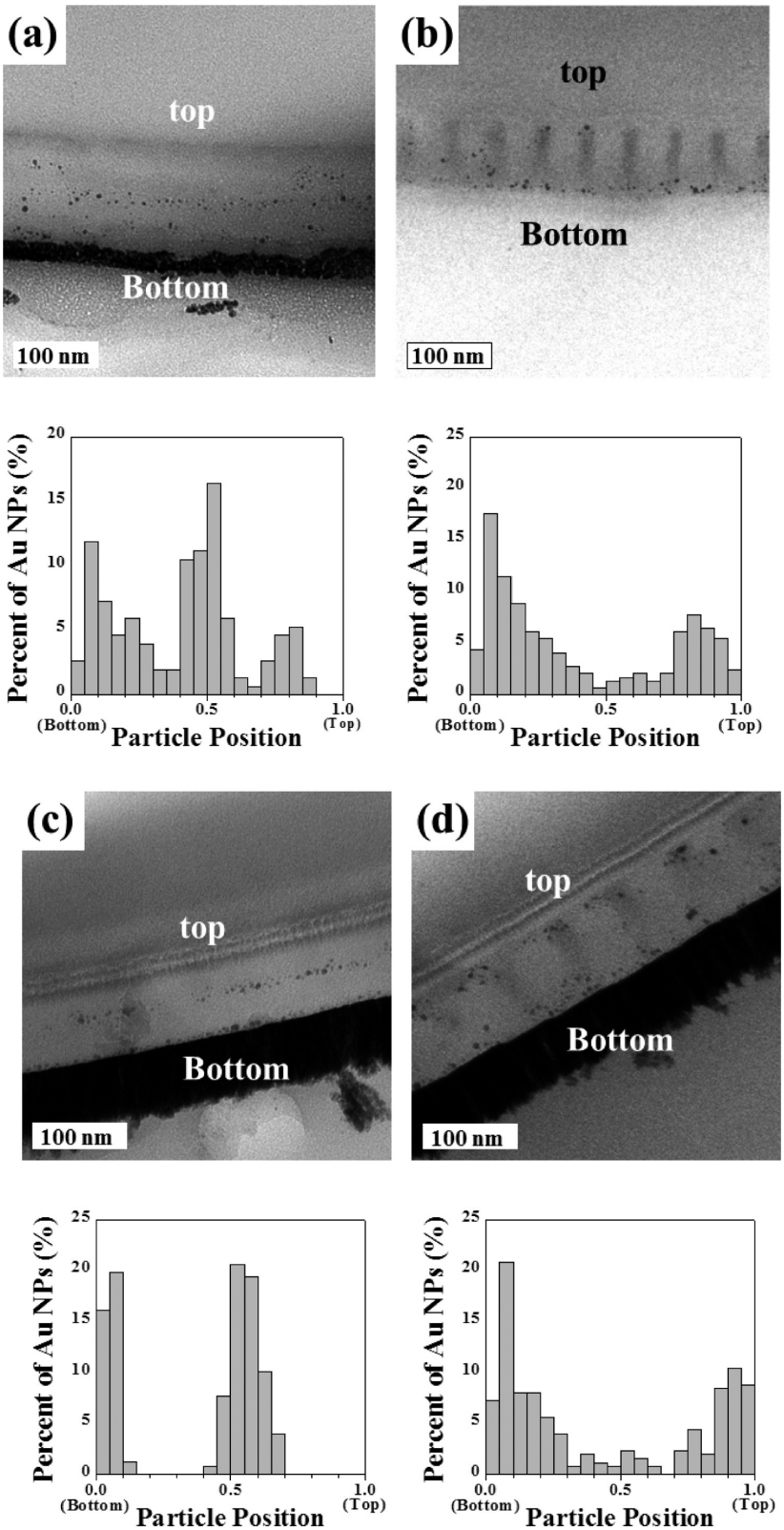

Figure 6. Cross-sectional TEM images and the corresponding histograms of nanoparticle location in PS-*b*-PMMA (M_n = 94 kg/mol) nanocomposite thin films containing 10 wt % of (a) Au NP-1 and (b) Au NP-3 and PS-*b*-PMMA (M_n = 130 kg/mol) nanocomposite thin films containing 10 wt % of (c) Au NP-1 and (d) Au NP-3. PMMA domains are stained selectively by OsO_4.

different particle positions.[52,53,55,56,62] (see Supporting Information for details) SCFT simulations were performed for both perpendicular- and parallel-oriented lamellae with a particle located as shown in Figure 7. We assumed that particles and

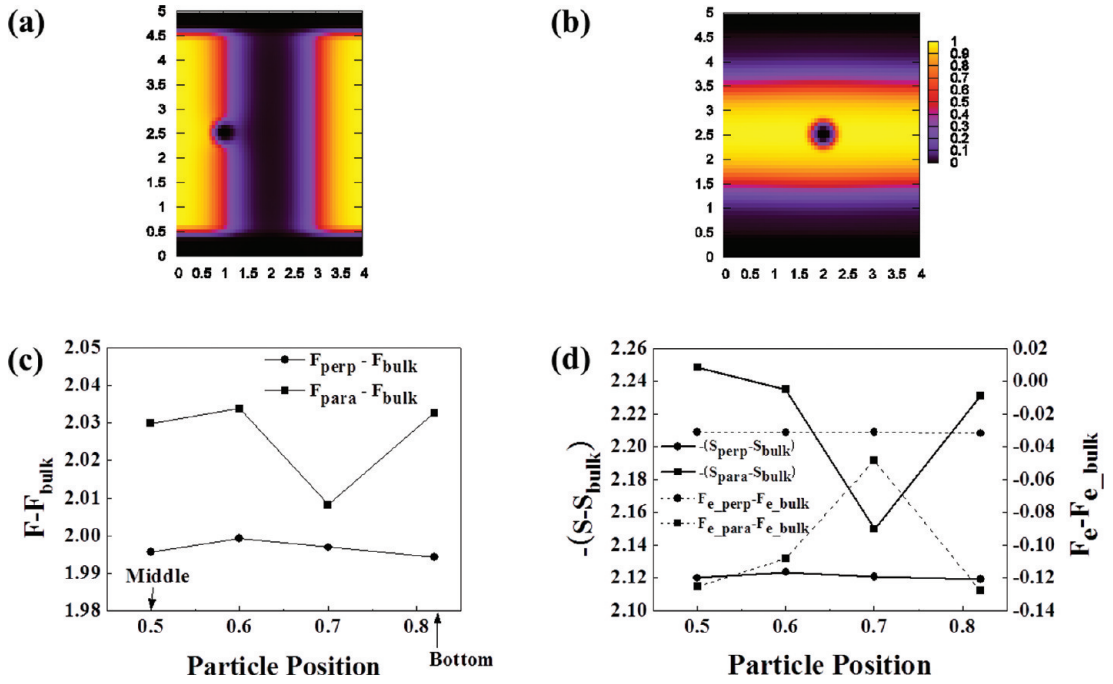

Figure 7. Numerical SCFT results. Volume fraction plots of (a) perpendicular-oriented lamellae and (b) parallel-oriented lamellae. Dark parts in the middle represent neutral particles. (c) Free energies according to relative particle positions. Values of relative particle positions, 1 and 0, are defined as the bottom and the top positions of the simulation box, respectively. (d) Entropy loss caused by particles and interaction energies, F_e, according to particle positions. The main portion of F_e is the enthalpic interaction.

walls are the same species and neutral to diblock copolymer segments. Free energies for the different particle positions are shown in Figure 7c. Consistent with the experimental results, as a particle approaches the wall, the free energy of the perpendicular-oriented lamellae decreases, reaching a minimal value when the particle is adjacent to the wall. Figure 7d shows entropy caused by particles as well as enthalpic (χN) interaction energy. The latter does not depend on particle positions for the perpendicular case since a particle is always located at the interface between two dissimilar segments. An increase in entropy comes from the fact that there are fewer neighboring block copolymer chains around a particle when the particle is adjacent to the wall, and this increase in entropy causes an attraction between the wall and the particle. Therefore, the neutral NPs are located at the interface of two dissimilar blocks and at the surface of the substrate to reduce the interfacial energy between two dissimilar blocks as well as the entropy loss of the block copolymer polymer chains near the particle. The Au NPs-3 also partially neutralize the interactions of the substrate with the different block copolymer domains, thus further facilitating the perpendicular orientation of the lamellae. These SCFT results are consistent with the previous findings of Balazs et al.[49]

■ CONCLUSIONS

In this study, we developed a general strategy for controlling the orientation of microdomains in AB diblock copolymer thin films by introducing Au NPs whose surfaces are either neutral for the AB domains or selective for either A or B. To impart thermal stability and tune the surface properties of the Au NPs, their surface was modified with polymeric ligand, P[(MMA-*r*-S)-*b*-S-N_3]-SH. The MMA and styrene composition in P(MMA-*r*-S) were adjusted to control the interfacial interaction between Au NPs and the PS-*b*-PMMA block copolymer. We successfully synthesized Au NPs that were selective to the PMMA domain and neutral Au NPs that were localized to the PS/PMMA interface in the PS-*b*-PMMA bulk after thermal annealing. These two types of Au NPs were introduced to the PS-*b*-PMMA thin films and the resulting orientation of the nanocomposite thin films was remarkably dependent on the type and content of Au NPs. The PS-*b*-PMMA nanocomposite thin films including the selective Au NPs produced a parallel orientation to the substrate regardless of the amount of Au NPs. In contrast the PS-*b*-PMMA nanocomposite thin films that contained 5 wt % or more of neutral Au NPs were oriented perpendicularly, whereas the thin films containing a low content of neutral Au NPs still exhibited a parallel orientation. We also examined the lateral and vertical location of the Au NPs in the PS-*b*-PMMA thin films using top-view and cross-sectional TEM. From the top-view TEM images, it was observed that the neutral Au NPs were dispersed throughout the entire sample with slight segregation of the Au NPs at the PS/PMMA interface. In the vertical direction, the neutral Au NPs were mainly located near the substrate with some near the top surfaces. SCFT simulations show that neutral Au NPs at the PS/PMMA interface can move to the substrate to reduce the entropic penalty of the block polymer chains. They also neutralize the surface of the substrate, thereby resulting in the perpendicular orientation of block copolymer lamellar domains. Finally, these results provide a simple route for fabricating well-defined nanocomposites films with precise control of microdomain orientation as well as NP location within block copolymer templates.

■ ASSOCIATED CONTENT

Supporting Information. Additional synthesis, NMR, TEM, GISAXS, and SFM images and a discussion of the self-

consistent-field theory simulations. This material is available free of charge via the Internet at http://pubs.acs.org.

AUTHOR INFORMATION

Corresponding Author

*E-mail: (J.B.) joona@korea.ac.kr; (B.J.K.) bumjoonkim@kaist.ac.kr; (W.B.L.) wblee92@sogang.ac.kr.

ACKNOWLEDGMENT

This work was supported by the Korea Research Foundation Grant funded by the Korean Government (MOEHRD) (2011-0002748) and also by the Human Resources Development Program of KETEP grant (No. 20114010203070) funded by the Korea government Ministry of Knowledge Economy. The work at UCSB was supported by the MRSEC Program of the National Science Foundation under Award DMR-1121053.

REFERENCES

(1) Bang, J.; Jeong, U.; Ryu, D. Y.; Russell, T. P.; Hawker, C. J. *Adv. Mater.* **2009**, *21*, 4769.
(2) Hamley, I. W. *Prog. Polym. Sci.* **2009**, *34*, 1161.
(3) Hawker, C. J.; Russell, T. P. *MRS Bull.* **2005**, *30*, 952.
(4) Kim, H. C.; Park, S. M.; Hinsberg, W. D. *Chem. Rev.* **2010**, *110*, 146.
(5) Stoykovich, M. P.; Nealey, P. F. *Mater Today* **2006**, *9*, 20.
(6) Cheng, J. Y.; Ross, C. A.; Thomas, E. L.; Smith, H. I.; Vancso, G. J. *Adv. Mater.* **2003**, *15*, 1599.
(7) Hammond, M. R.; Cochran, E. W.; Fredrickson, G. H.; Kramer, E. J. *Macromolecules* **2005**, *38*, 6575.
(8) Segalman, R. A.; Schaefer, K. E.; Fredrickson, G. H.; Kramer, E. J.; Magonov, S. *Macromolecules* **2003**, *36*, 4498.
(9) Cheng, J. Y.; Rettner, C. T.; Sanders, D. P.; Kim, H. C.; Hinsberg, W. D. *Adv. Mater.* **2008**, *20*, 3155.
(10) Ruiz, R.; Kang, H. M.; Detcheverry, F. A.; Dobisz, E.; Kercher, D. S.; Albrecht, T. R.; de Pablo, J. J.; Nealey, P. F. *Science* **2008**, *321*, 936.
(11) Hong, A. J.; Liu, C. C.; Wang, Y.; Kim, J.; Xiu, F. X.; Ji, S. X.; Zou, J.; Nealey, P. F.; Wang, K. L. *Nano Lett.* **2010**, *10*, 224.
(12) Thurn-Albrecht, T.; Schotter, J.; Kastle, C. A.; Emley, N.; Shibauchi, T.; Krusin-Elbaum, L.; Guarini, K.; Black, C. T.; Tuominen, M. T.; Russell, T. P. *Science* **2000**, *290*, 2126.
(13) Kim, M.; Safron, N. S.; Han, E.; Arnold, M. S.; Gopalan, P. *Nano Lett.* **2010**, *10*, 1125.
(14) Jung, J. M.; Kwon, K. Y.; Ha, T. H.; Chung, B. H.; Jung, H. T. *Small* **2006**, *2*, 1010.
(15) Phillip, W. A.; O'Neill, B.; Rodwogin, M.; Hillmyer, M. A.; Cussler, E. L. *ACS Appl. Mater. Inter.* **2010**, *2*, 847.
(16) Fan, H. J.; Werner, P.; Zacharias, M. *Small* **2006**, *2*, 700.
(17) Jung, H.; Hwang, D.; Kim, E.; Kim, B. J.; Lee, W. B.; Poelma, J. E.; Kim, J.; Hawker, C. J.; Huh, J.; Ryu, D. Y.; Bang, J. *ACS Nano* **2011**, *5*, 6164.
(18) Gonsalves, K. E.; Merhari, L.; Wu, H. P.; Hu, Y. Q. *Adv. Mater.* **2001**, *13*, 703.
(19) Maity, A.; Biswas, M. *J Ind. Eng. Chem.* **2006**, *12*, 311.
(20) Schaefer, D. W.; Justice, R. S. *Macromolecules* **2007**, *40*, 8501.
(21) Vaia, R. A.; Maguire, J. F. *Chem. Mater.* **2007**, *19*, 2736.
(22) Reddy, B. *Advances in Diverse Industrial Applications of Nanocomposites*; InTech: 2011.
(23) Balazs, A. C.; Emrick, T.; Russell, T. P. *Science* **2006**, *314*, 1107.
(24) Al Akhrass, S.; Gal, F.; Damiron, D.; Alcouffe, P.; Hawker, C. J.; Cousin, F.; Carrot, G.; Drockenmuller, E. *Soft Matter* **2009**, *5*, 586.
(25) Al Akhrass, S.; Damiron, D.; Carrot, G.; Drockenmuller, E. *J. Polym. Sci., Part A: Polym. Chem.* **2010**, *48*, 3888.
(26) Lee, S.; Lee, B.; Kim, B. J.; Park, J.; Yoo, M.; Bae, W. K.; Char, K.; Hawker, C. J.; Bang, J.; Cho, J. H. *J. Am. Chem. Soc.* **2009**, *131*, 2579.
(27) Mezzenga, R.; Ruokolainen, J. *Nat. Mater.* **2009**, *8*, 926.
(28) Son, J. G.; Bae, W. K.; Kang, H. M.; Nealey, P. F.; Char, K. *ACS Nano* **2009**, *3*, 3927.
(29) Neouze, M. A.; Schubert, U. *Monatsh. Chem.* **2008**, *139*, 183.
(30) Shan, J.; Tenhu, H. *Chem. Commun.* **2007**, 4580.
(31) Zou, H.; Wu, S.; Shen, J. *Chem. Rev.* **2008**, *108*, 3893.
(32) Lin, Y.; Boker, A.; He, J.; Sill, K.; Xiang, H.; Abetz, C.; Li, X.; Wang, J.; Emrick, T.; Long, S.; Wang, Q.; Balazs, A.; Russell, T. P. *Nature* **2005**, *434*, 55.
(33) Yeh, S. W.; Wei, K. H.; Sun, Y. S.; Jeng, U. S.; Liang, K. S. *Macromolecules* **2005**, *38*, 6559.
(34) Corbierre, M. K.; Cameron, N. S.; Sutton, M.; Laaziri, K.; Lennox, R. B. *Langmuir* **2005**, *21*, 6063.
(35) Corbierre, M. K.; Cameron, N. S.; Sutton, M.; Mochrie, S. G. J.; Lurio, L. B.; Rühm, A.; Lennox, R. B. *J. Am. Chem. Soc.* **2001**, *123*, 10411.
(36) Park, S. C.; Kim, B. J.; Hawker, C. J.; Kramer, E. J.; Bang, J.; Ha, J. S. *Macromolecules* **2007**, *40*, 8119.
(37) Xu, C.; Ohno, K.; Ladmiral, V.; Milkie, D. E.; Kikkawa, J. M.; Composto, R. J. *Macromolecules* **2009**, *42*, 1219.
(38) Kwon, T.; Min, M.; Lee, H.; Kim, B. J. *J. Mater. Chem.* **2011**, *21*, 11956.
(39) Paek, K.; Chung, S.; Cho, C.-H.; Kim, B. J. *Chem. Commun.* **2011**, *47*, 10272.
(40) Kang, D. J.; Kwon, T.; Kim, M. P.; Cho, C.-H.; Jung, H.; Bang, J.; Kim, B. J. *ACS Nano* **2011**, DOI: 10.1021/nn203209c.
(41) Kim, B. J.; Bang, J.; Hawker, C. J.; Chiu, J. J.; Pine, D. J.; Jang, S. G.; Yang, S. M.; Kramer, E. J. *Langmuir* **2007**, *23*, 12693.
(42) Kim, B. J.; Bang, J.; Hawker, C. J.; Kramer, E. J. *Macromolecules* **2006**, *39*, 4108.
(43) Chiu, J. J.; Kim, B. J.; Kramer, E. J.; Pine, D. J. *J. Am. Chem. Soc.* **2005**, *127*, 5036.
(44) Chiu, J. J.; Kim, B. J.; Yi, G. R.; Bang, J.; Kramer, E. J.; Pine, D. J. *Macromolecules* **2007**, *40*, 3361.
(45) Kim, B. J.; Fredrickson, G. H.; Hawker, C. J.; Kramer, E. J. *Langmuir* **2007**, *23*, 7804.
(46) Kim, B. J.; Fredrickson, G. H.; Kramer, E. J. *Macromolecules* **2008**, *41*, 436.
(47) Jang, S. G.; Khan, A.; Dimitriou, M. D.; Kim, B. J.; Lynd, N. A.; Kramer, E. J.; Hawker, C. J. *Soft Matter* **2011**, *7*, 6255.
(48) Kim, B. J.; Fredrickson, G. H.; Bang, J.; Hawker, C. J.; Kramer, E. J. *Macromolecules* **2009**, *42*, 6193.
(49) Lee, J. Y.; Shou, Z. Y.; Balazs, A. C. *Macromolecules* **2003**, *36*, 7730.
(50) Yoo, M.; Kim, S.; Lim, J.; Kramer, E. J.; Hawker, C. J.; Kim, B. J.; Bang, J. *Macromolecules* **2010**, *43*, 3570.
(51) Lim, J.; Yang, H.; Paek, K.; Cho, C.-H.; Kim, S.; Bang, J.; Kim, B. J. *J. Polym. Sci., Part A: Polym. Chem.* **2011**, *49*, 3464.
(52) Matsen, M. W.; Schick, M. *Phys. Rev. Lett.* **1994**, *72*, 2660.
(53) Fredrickson, G. H.; Helfand, E. *J. Chem. Phys.* **1987**, *87*, 697.
(54) Leibler, L. *Macromolecules* **1980**, *13*, 1602.
(55) Fredrickson, G. H. *The equilibrium theory of inhomogeneous polymers*; Oxford University Press: Oxford, U.K., 2006.
(56) Cochran, E. W.; Garcia-Cervera, C. J.; Fredrickson, G. H. *Macromolecules* **2006**, *39*, 2449.
(57) Torikai, A.; Hozumi, A.; Fueki, K. *Polym. Degrad. Stab.* **1986**, *16*, 13.
(58) Bang, J.; Bae, J.; Lowenhielm, P.; Spiessberger, C.; Given-Beck, S. A.; Russell, T. P.; Hawker, C. J. *Adv. Mater.* **2007**, *19*, 4552.
(59) Brust, M.; Walker, M.; Bethell, D.; Schiffrin, D. J.; Whyman, R. *J. Chem. Soc., Chem. Commun.* **1994**, 801.
(60) Mansky, P.; Liu, Y.; Huang, E.; Russell, T. P.; Hawker, C. J. *Science* **1997**, *275*, 1458.
(61) Ryu, D. Y.; Shin, K.; Drockenmuller, E.; Hawker, C. J.; Russell, T. P. *Science* **2005**, *308*, 236.
(62) Sides, S. W.; Kim, B. J.; Kramer, E. J.; Fredrickson, G. H. *Phys. Rev. Lett.* **2006**, *96*, 250601.